# 8 Ca$^+$–X and Y–Ca$^+$–X Complexes Important in the Chemistry of Ionospheric Calcium (X = H$_2$O, CO$_2$, N$_2$, O$_2$ and O)

## 8.1 Introduction

Ca$^+$ is unusual for a meteoric metal ion in that it can be observed by LIDAR (light detection and ranging). This is not possible for other metal ions as their resonance transitions are in the UV, well below 300 nm: such radiation is therefore absorbed by stratospheric O$_3$. The chemistry of Ca$^+$ is thought to be similar[1] to that of Mg$^+$ and it is thought that it could be used to study sporadic E layers (E$_s$) of which metal ions, and in particular Mg$^+$ and Fe$^+$, are major constituents.

As discussed in detail in Chapter 1 evidence suggests that neutralization of Ca$^+$ in these sporadic E layers occurs through a number of ligand exchange reactions followed by dissociative recombination, and is responsible for the phenomenon of sporadic neutral metal layers (M$_s$) in the MLT region of the atmosphere. The simultaneous observation of calcium cations and calcium in E$_s$ and M$_s$ respectively would be extremely useful in determining the reliability of theoretical models in these situations, giving confidence in models for which only the neutral species can be observed.

In the present study, *ab initio* calculations are reported for the intermediate complexes, X–Ca$^+$–Y of ligand-exchange reactions that

are expected to occur in this region of the atmosphere, as described in Chapter 1. The energy of the intermediate complex relative to the X + $Ca^+$–Y and Y + $Ca^+$–X asymptotes in the ligand-exchange reaction is required to enable the calculation of the corresponding rate constants by the use of (Rice-Ramsperger-Kassell-Marcus) RRKM theory, together with the rovibrational energy levels (obtained from the rotational constants and the vibrational frequencies). These RRKM calculations, are performed by Professor John Plane at the University of Leeds, and should provide insight into the competition between ligand-exchange reactions (some of which can lead back to $Ca^+$, for which neutralization is inefficient) and dissociative recombination of the complexes. The results that are obtained in the present study have been employed in atmospheric modelling and published in an article,[2] and are an extension of a recent experimental study by Plane and co-workers.[3]

## 8.2  Calculational details

Calculations were carried out using the GAUSSIAN 03 suite of programs[4] on intermediate cluster ions of the type X–$Ca^+$–Y, which are formed during expected and postulated ligand-switching reactions in the MLT region, in order to obtain binding energies, harmonic vibrational frequencies and rotational constants. Preliminary Hartree-Fock (HF) optimizations with Pople 6-311+G(2d, p) triple-zeta basis sets were performed to gain approximate initial geometries, and then further B3LYP and MP2 geometry optimizations and vibrational frequency calculations using the same basis sets were performed.

RCCSD(T) single point calculations were then carried out employing MOLPRO[5] at the B3LYP and MP2 optimized geometries. Basis sets employed in the RCCSD(T) calculations were the standard Dunning aug-cc-pVQZ basis sets for first-row elements, while for Ca the cc-pVQZ basis set[6] was employed, to which further diffuse $s$, $p$, $d$, $f$ and $g$ functions were added in an even-tempered expansion of the two most diffuse functions of each orbital angular momentum type. The frozen-core approximation was used in which the only the valence electrons were included in the correlation treatment, although in the RCCSD(T) calculations, only the calcium $1s$, $2s$ and $2p$ orbitals and the N, O and C $1s$ orbitals were kept in the core.

To perform a geometry optimization using the high level RCCSD(T) method for these systems would be incredibly time consuming and so optimizations are carried out using the MP2 and B3LYP methods. The idea of using both MP2 and B3LYP is to enable a comparison between geometries obtained from two differing methods. It is expected both these methods will give a good estimate for the geometries from which the RCCSD(T) calculations will be able to determine accurate dissociation energies (as discussed in section 3.4.3). It is worth noting that in previous, similar[24] studies optimized geometries, determined at the B3LYP and MP2 levels of theory, have compared very well to the geometries, obtained at the QCISD level of theory. Although, as previously mentioned in section 3.4.3, it is difficult to give a detailed assessment of the accuracy at a given level of theory,[7] where possible comparison is made to values determined experimentally via mass spectrometric studies, photodissociation experiments and guided ion-

beam studies.  In general, the results obtained are found to be in very good agreement with these experimental results (within experimental error) giving confidence in the computational methods used.

### 8.3  *Ab initio calculations on Ca⁺-X complexes*

Recently, Broadley *et al.*[3] presented the results of B3LYP/6-311+G(2d,p) calculations on the complexes of $Ca^+$ with a single ligand. They reported optimized geometries, harmonic vibrational frequencies and dissociation energies, $D_0$.  As part of the present work, these structures were confirmed, following which, single-point RCCSD(T)/aug-cc-pVQZ calculations were performed to determine more accurate dissociation energies.  The results are shown in Table 8.1, where $D_0$ values have been obtained by making use of the B3LYP/6-311+G(2d,p) harmonic vibrational frequencies reported in reference 3 and confirmed herein.

#### 8.3.1  $CaO_2^+$

For $CaO_2^+$, geometry optimizations were performed on linear and $C_{2v}$ structures, with the complex in both the doublet and quartet state. The lowest state was the $C_{2v}$ structure with a $^2A_2$ electronic state, in agreement with the results of reference 3.  A value of $D_0$ for $CaO_2^+$ may be obtained from an estimate of the $CaO_2$ ionization energy of 567.33 $\pm$ 19.30 kJ mol$^{-1}$,[8] and a bond dissociation energy $D_0(Ca\text{-}O_2) = 225.78 \pm$ 16.40 kJ mol$^{-1}$,[8] yielding $D_0(Ca^+\text{–}O_2) = 250.86 \pm 16.40$ kJ mol$^{-1}$. This value is consistent with the present and previously-calculated[3] results shown in Table 8.1.

**Table 8.1. Dissociation energies (kJ mol⁻¹) for Ca⁺–X complexes (X = $H_2O$, $CO_2$, $N_2$, O and $O_2$).**

| Level of Theory | Speices | | | | |
| --- | --- | --- | --- | --- | --- |
| | Ca⁺–$H_2O$ | Ca⁺–$CO_2$ | Ca⁺–$N_2$ | CaO⁺ [a] | CaO$_2$⁺ |
| B3LYP/6-311++G(2d,p) | 115 | 54 | 22 | 341 | 223 |
| RCCSD(T)/aug-cc-pVQZ | 111.1 | 58.2 | 23.1 | 317.2 | 226.5 |
| Previous Theoretical. | 105[9] | | 21[11] | 313[15] | 250±30[8] |
| | | | 25[12] | 317[19] | |
| Experiment/ Do | 117[9] | >> 8[13] | 21±6[10] | 344±5[20] | |
| | | | | 318±10[21] | |

[a] $^2\Sigma^+$ state.

### 8.3.2 Ca⁺–$H_2O$

For Ca⁺–$H_2O$, an experimental $D_0$ value of 117 kJ mol⁻¹ has been obtained by Kochanski and Constantin[9] from mass spectrometric studies. The results of HF calculations with small basis sets were also reported in that work, giving a value of 105 kJ mol⁻¹, which is (perhaps surprisingly) in fair agreement with the previous B3LYP calculations,[3] and the present RCCSD(T) ones shown in Table 8.1. Thus, overall there is good agreement between experiment and theory.

### 8.3.3 Ca⁺$N_2$

For Ca⁺–$N_2$, Duncan and coworkers[10] obtained a spectroscopic value for the ground state dissociation energy of 21 ± 6 kJ mol⁻¹. This value was calculated from the Ca⁺ $^2P_{1/2} \leftarrow ^2S_{1/2}$ atomic transition and the $^2\Pi_{1/2}$ excited state dissociation energy determined through photodissociation experiments. This experimental value can be seen to be in excellent agreement with the value obtained herein, as well as with the previous B3LYP value[3] all of which are reported in Table 8.1. In a separate study, Duncan and coworkers[11] report a series of

calculations, obtaining a "best" value of $D_0$ of ~21 kJ mol^{-1} at the B3LYP level, in excellent agreement with both their previous experimental result, and the present results. Subsequent to that, Rodriguez-Santiago and Bauschlicher calculated a value of 25 kJ mol^{-1} at the MRCI+Q level, [12] slightly above the present calculated value, but still within the experimental error range of reference 10.

### 8.3.4  Ca^{+}–CO_2

For Ca^{+}–$CO_2$, a spectroscopic value for the ground state dissociation energy, determined in a similar fashion to that of Ca^{+}–$N_2$, of 669 cm^{-1} (8 kJ mol^{-1}) has been reported,[13] however, this was thought by the authors of reference 12 to be a lower bound, with the true value being much higher than this — a conclusion in line with the very much larger calculated values of 58.2 and 54 kJ mol^{-1} from the present and previous[3] work respectively (Table 8.1).

### 8.3.5  Ca^{+}O

The ground state of CaO[+] was determined in reference 3 to be $^2\Sigma^+$ which was consistent with the original findings of the present work published in reference 14.  However, subsequent calculations have suggested that there is a $^2\Pi$ state that is likely to lie lower in energy as reported in reference 15.  This $^2\Pi$ state arises owing to the unpaired electron on the oxygen being located perpendicular the internuclear axis, in either the O $p_x$ or $p_y$ orbital, whilst for the $^2\Sigma^+$ state the unpaired electron is located along the internuclear axis in the O $p_z$ orbital.  To complicate matters, work[16,17,18] on the valence isoelectronic

species NaO found the excited $A^2\Sigma^+$ state, that lies ~2000 cm$^{-1}$ above the $X^2\Pi$ electronic ground state, is formed preferentially in the Na + O$_3$ atmospheric gas phase reaction with a branching ratio to the $X^2\Pi$ state of at least 2:1. The overall implications (if any) of Ca$^+$O having an $X^2\Pi$ electronic ground state on the work herein and subsequent work is not known. However, it is clear that further work is required to determine the predominant state of Ca$^+$O formed in the MLT region for inclusion in subsequent atmospheric models.

Discussing the dissociation energy, $D_0$, assuming as discussed above a $^2\Sigma^+$ ground state, there is reasonable agreement between the B3LYP results of Broadley *et al.*[3] and the present RCCSD(T) results, with the RCCSD(T) value being *ca.* 24 kJ mol$^{-1}$ smaller. The latter value is, however, in excellent agreement with previous RCCSD(T) results from Harrison *et al.,*[15] with the present calculation employing a larger basis set, and in almost perfect agreement with a previous CI value from Partridge *et al.*[19] There is an experimental value of 344 ± 4 kJ mol$^{-1}$ determined from a guided ion-beam experiment by Fisher *et al.,*[20] which is larger than the present RCCSD(T) and previous theoretical results, but is in good agreement with the B3LYP results. In addition, there is good agreement with the earlier mass spectrometric result of Murad.[21]

### 8.4  Geometries of intermediate complexes

*8.4.1  Intermediate complexes involving closed shell species*

As discussed previously in Chapter 1, three closed shell ligands are considered to be important in the $Y + Ca^+–X \leftrightarrow X–Ca^+–Y \leftrightarrow Ca^+–Y + X$ (where X, Y = $CO_2$, $N_2$ and $H_2O$) ligand switching reaction which occur in the upper atmosphere.   Hence, there are three intermediate complexes in which the open-shell atomic cation $Ca^+$ would be complexed solely by two different closed-shell species.   A general assumption is that, because of steric and electrostatic interactions, the two species would approach the cationic metal from opposite sides, but the manner in which they approach still allows for a number of possible structures for each of the three pairs of ligands. For $H_2O$, the approach is assumed to be with the δ- oxygen atom pointing towards the $Ca^+$ with the hydrogens pointing away.  $CO_2$ has the potential to approach the $Ca^+$ either end-on, with one of the electronegative oxygens interacting with the calcium cation, or side-on, allowing both oxygen atoms to interact.   In this investigation the side-on approach has not been considered since previous experience[22,23] has shown it is higher in energy both because of the repulsive interaction between the δ+ carbon atom and the cation, and the large energy required to bend the $CO_2$ molecule.  Similarly, $N_2$ has the possibility of approaching either end- or side-on, although in this case the preferential approach of the ligand is less clear because of its large negative quadrupole moment, hence calculations of both approaches were performed.   In view of these assumptions only one structure for $CO_2–Ca^+–H_2O$ has been considered while for both

$CO_2$-$Ca^+$–$N_2$ and $H_2O$–$Ca^+$–$N_2$ two structures have been considered. In both cases the two structures are a result of the possibility of the $N_2$ approaching in either an end- or side-on manner. The results of these calculations are presented in Table 8.2 and Table 8.3, with the optimized geometries shown in Figure 8.1.

**Table 8.2. Total energies, electronic states and harmonic vibrational frequencies for X–$Ca^+$–Y complexes (where X and Y = $CO_2$, $N_2$ and $H_2O$) calculated at MP2/6-311++G (2d,p) level of theory. Note that $N_2$(s) indicates $N_2$ approaching in a side-on manner, whilst *i* indicates an imaginary frequency. The global minima are highlighted.**

| X | Y | State | Energy ($E_h$) | Vibrational frequencies ($cm^{-1}$) |
|---|---|---|---|---|
| $CO_2$ | $N_2$ | $^2\Sigma^+$ | -974.340272 | 23($\pi$), 23($\pi$), 59($\pi$), 59($\pi$), 84($\sigma$), 139($\pi$), 139($\pi$), 183($\sigma$), 636($\pi$), 636($\pi$), 1324($\sigma$), 2402($\sigma$), 2415($\sigma$) |
| $CO_2$ | $N_2$(s) | $^2A_1$ | -974.334738 | 64*i*($b_2$), 4($b_2$), 5($b_1$), 17($a_1$), 62($b_2$), 62($b_1$), 172($a_1$), 638($b_1$), 639($b_2$), 1322($a_1$), 2168($a_1$), 2414($a_1$) |
| $CO_2$ | $H_2O$ | $^2A_1$ | -941.340056 | 328($b_1$), 416($b_2$), 637($b_1$), 637($b_2$), 1325($a_1$), 1649($a_1$), 2415(a1), 3749(a1), 3851(b2) |
| $H_2O$ | $N_2$ | $^2A_1$ | -862.408114 | 33($b_1$), 36($b_2$), 91($a_1$), 138($b_1$), 140($b_2$), 300($a_1$), 337($b_1$), 424($b_2$), 1651($a_1$), 2392($a_1$), 3748($a_1$), 3848($b_2$) |
| $H_2O$ | $N_2$(s) | $^2A_1$ | -862.402765 | 64*i*($b_2$), 4($a_2$), 5($b_2$), 7($b_1$), 18($a_1$), 293($a_1$), 372($b_1$), 447($b_2$), 1660($a_1$), 2168($a_1$), 3751($a_1$), 3846($b_2$) |

From Tables 8.2 and 8.3 it can be seen that in each case an end-on approach of the $N_2$ is favoured by all ligands. In the case of $CO_2$–$Ca^+$–$N_2$, this results in a linear structure ($C_{\infty v}$); for $CO_2$–$Ca^+$–$H_2O$ and $N_2$–$Ca^+$–$H_2O$, this results in a structure in which only the two hydrogens lie off the principal axis ($C_{2v}$). The less favourable side-on approach of the $N_2$ is indicated by the higher energy in each of these two structures in comparison to those formed by an end-on approach. Imaginary frequencies found by a vibrational frequency analysis, for those complexes formed by a side-on approach suggest that they are

located at saddle points on the potential energy surface of both the associated complexes. The structures formed from an end-on approach of $N_2$ all exhibit only real frequencies and hence are at geometries which are believed to be the global minima. Agreement of both methodologies in the approach geometry of the $N_2$ ligand and in the general energies, states and frequencies yielded, gives confidence that the calculated lowest energy structures are the global minima.

**Table 8.3. Total energies, electronic states and harmonic vibrational frequencies for X–Ca$^+$–Y complexes (where X and Y = $CO_2$, $N_2$ and $H_2O$) calculated at B3LYP/6-311++G (2d,p) level of theory. Note that $N_2$(s) indicates $N_2$ approaching in a side-on manner, whilst _i_ indicates an imaginary frequency. The global minima are highlighted.**

| X | Y | State | Energy ($E_h$) | Vibrational frequencies (cm$^{-1}$) |
|---|---|---|---|---|
| $CO_2$ | $N_2$ | $^2\Sigma^+$ | -975.594423 | 26($\pi$), 26($\sigma$), 64($\pi$), 64($\pi$), 120($\sigma$), 152($\pi$), 152($\pi$), 213($\sigma$), 642($\pi$), 642($\pi$), 1370.6($\sigma$), 2428($\sigma$), 2447($\sigma$) |
| $CO_2$ | $N_2$(s) | $^2A_1$ | -975.584946 | 71$i$($b_2$), 5$i$($b_1$), 3($b_2$), 8($a_1$), 63($b_2$), 63($b_1$), 198($a_1$), 643($b_1$), 644($b_2$), 1367($a_1$), 2427($a_1$), 2431($a_1$) |
| $CO_2$ | $H_2O$ | $^2A_1$ | -942.524759 | 32($b_1$), 33($b_2$), 67($b_1$), 69($b_2$), 165($a_1$), 320($a_1$), 325($b_1$), 420($b_2$), 643($b_2$), 644($b_1$), 1369($a_1$) , 1650($a_1$), 2425($a_1$), 3729 ($a_1$), 3812($b_2$) |
| $H_2O$ | $N_2$ | $^2A_1$ | -863.427426 | 34($b_1$), 35($b_2$), 126($a_1$), 140($b_1$), 143($b_2$), 314($a_1$), 330($b_1$), 427($b_2$), 1651($a_1$), 2446($a_1$), 3729($a_1$), 3810($b_2$) |
| $H_2O$ | $N_2$(s) | $^2A_1$ | -863.418865 | 67$i$($b_2$), 41$i$($a_2$), 12$i$($b_1$), 5$i$($b_2$), 6($a_1$), 319($a_1$), 358($b_1$), 449($b_2$), 1657($a_1$), 2432($a_1$), 3722($a_1$), 3802($b_2$) |

## 8.4.2 _Geometries of O–Ca$^+$–X (where X is $CO_2$, $N_2$ or $H_2O$) intermediate complex ions_

The complexes of O–Ca$^+$–X (where X is $CO_2$, $N_2$ or $H_2O$) involve two open-shell species, O and Ca$^+$. This means that as well as considering the end-on versus side-on approaches that were discussed for Ca$^+$ interacting with only closed-shell ligands (again from either side of the

Ca$^+$) an overall quartet or doublet spin multiplicity is possible, as is the possibility of chemical bond formation. This can occur *via* a charge transfer from the Ca$^+$ to the O atom, leaving a double positive charge on the Ca and a single negative charge on the O. As implied above, for the Ca$^+$·O species the resulting doublet state formed is at a lower energy than the quartet state. For the complexes, calculations were performed for both the doublet and quartet states of all the structures considered, in which the same assumptions were made as for the complexes within the previous subsection: $H_2O$ approaches Ca$^+$ *via* its δ- oxygen, $CO_2$ approaches in an end-on manner, and $N_2$ approaches either in an end-on or side on manner. The calculations on these structures yielded minima for each of the structures with the exception of the O–Ca$^+$–$CO_2$ linear arrangement; examination of the imaginary frequencies from the calculations on the linear structure indicated that the minimum structure could be found by allowing the O and $CO_2$ to bend towards each other, breaking the $C_{\infty v}$ symmetry of the complex. Constraints in the geometry optimization were relaxed to allow the structure to optimize in this manner and a minimum was located. Further optimizations from different starting positions on the potential energy surface also found the same minimum. The results of these calculations are shown in Tables 8.4 and 8.5 with the geometries again shown in Figure 8.1.

It can be seen from Tables 8.4 and 8.5 that both methodologies calculate the doublet states to be of lower energy in energy than the quartet state consistent with the charge transfer between the Ca$^+$ and O. This is evinced by the spin and charge analyses, in which the

unpaired electron's spin appears to be largely centred on the O atom with the charges of the two species being consistent with $Ca^{2+}$ and $O^-$. Using the $N_2$–CaO$^+$ ($^2\Sigma^+$) complex as an example the respective spin densities for Ca$^+$ and O were 0.044 and 0.955 whilst the charge on the respective atoms were 1.980 and -0.868. It can also be seen from both Tables 8.4 and 8.5 and Figure 8.1 that, as before, an end-on approach by $N_2$ is preferred to that of a side-on approach, regardless of whether the complex in question is in its quartet or doublet spin state.

**Table 8.4.** **Total energies, electronic states and harmonic vibrational frequencies for OCa$^+$–Y complexes (where X = CO$_2$, N$_2$ and H$_2$O) calculated at MP2/6-311++G (2d,p) level of theory. Note that N$_2$(s) indicates N$_2$ approaching in a side-on manner, whilst *i* indicates an imaginary frequency. The global minima are highlighted.**

| X | Y | State | Energy ($E_h$) | Vibrational frequencies (cm$^{-1}$) |
|---|---|---|---|---|
| O | $CO_2$ | $^4\Sigma^-$ | -939.953153 | 29($\pi$), 29($\pi$), 66($\pi$), 66($\pi$), 113($\sigma$), 189($\sigma$), 638($\pi$), 638($\pi$), 1324($\sigma$), 2415($\sigma$) |
| O | $N_2$ | $^4\Sigma^-$ | -861.020397 | 31($\pi$), 31($\pi$), 91($\sigma$), 147($\sigma$), 148($\pi$), 148($\pi$), 2408($\sigma$) |
| O | $sN_2$ | $^4A_2$ | -860.338871 | 73$i$(b$_2$), 5(b$_2$), 6(b$_1$), 21(a$_1$), 130(a$_1$), 2167(a$_1$) |
| O | $H_2O$ | $^4A_2$ | -828.020893 | 38(b$_1$), 41(b$_2$), 123(a$_1$), 301(a$_1$), 351(b$_1$), 430(b$_2$), 1654(a$_1$), 3750(a$_1$), 3849(b$_2$) |
| O | $CO_2$ | $^2A'$ | -940.064957 | 26(a'), 77(a''), 91(a'), 216(a'), 597(a'), 640(a''), 640(a'), 1326(a'), 2420(a') |
| O | $N_2$ | $^2\Sigma^+$ | -861.125360 | 11($\pi$), 11($\pi$), 168($\sigma$), 174($\pi$), 174($\pi$), 661($\sigma$), 2192($\sigma$) |
| O | $sN_2$ | $^2B_1$ | -861.117203 | 148$i$(b$_2$), 10$i$(b$_1$), 9(b$_2$), 98(a$_1$), 608(a$_1$), 2152(a$_1$) |
| O | $H_2O$ | $^2A''$ | -828.134702 | 59(a'), 172(a''), 339(a'), 402(a''), 493(a'), 589(a'), 1649(a'), 3752(a'), 3866(a') |

**Table 8.5.** **Total energies, electronic states and harmonic vibrational frequencies for OCa$^+$–X complexes (where X = CO$_2$, N$_2$ and H$_2$O) calculated at B3LYP/6-311++G (2d,p) level of theory. Note that N$_2$(s) indicates N$_2$ approaching in a side-on manner, whilst *i* indicates an imaginary frequency. The global minima are highlighted.**

| X | Y | State | Energy ($E_h$) | Vibrational frequencies (cm$^{-1}$) |
|---|---|---|---|---|
| O | CO$_2$ | $^4\Sigma^-$ | -941.122133 | 34($\pi$), 34($\pi$), 71($\pi$), 71($\pi$), 144($\sigma$), 216($\sigma$), 643($\pi$), 643($\pi$), 1369($\sigma$), 2427($\sigma$) |
| O | N$_2$ | $^4\Sigma^-$ | -862.023816 | 38($\pi$), 38($\pi$), 129($\sigma$), 154($\pi$), 154($\pi$), 191($\sigma$), 2446($\sigma$) |
| O | sN$_2$ | $^4A_2$ | -862.013479 | 86$i$(b$_2$), 11(a$_1$), 19(b$_1$), 20(b$_2$), 162(a$_1$), 2430(a$_1$) |
| O | H$_2$O | $^4A_2$ | -828.955232 | 43(b$_1$), 46(b$_2$), 154(a$_1$), 320(a$_1$), 341(b$_1$), 434(b$_2$), 1653(a$_1$), 3729(a$_1$), 3809(b$_2$) |
| O | CO$_2$ | $^2A'$ | -941.249598 | 41(a'), 83(a''), 94(a'), 213(a'), 615(a'), 652(a'), 653(a''), 1369(a'), 2432(a') |
| O | N$_2$ | $^2\Sigma^+$ | -862.144395 | 71($\pi$), 71($\pi$), 161($\sigma$), 165($\pi$), 165($\pi$), 675($\sigma$), 2445($\sigma$) |
| O | sN$_2$ | $^2B_1$ | -862.137776 | 147$i$(b$_2$), 51$i$(b$_1$), 48$i$(b$_2$), 87(a$_1$), 623(a$_1$), 2417(a$_1$) |
| O | H$_2$O | $^2A''$ | -829.083398 | 60(a'), 67(a''), 333(a'), 388(a''), 487(a'), 606(a'), 1661(a'), 3752(a'), 3837(a') |

*8.4.3 Geometries of O$_2$Ca$^+$–X (where X = CO$_2$, N$_2$ or H$_2$O) intermediate complex ions.*

Like O, O$_2$ is open-shell in its neutral ground state (X$^3\Sigma_g^-$) and therefore similar considerations for the O$_2$–Ca$^+$–X complexes have to be made as for the O–Ca$^+$–X species, in particular the possibility that an electron can be donated from Ca$^+$ to O$_2$. An additional consideration for O$_2$ is that, like N$_2$, this ligand can approach the complex in either a side-on or end-on manner. Previous calculations have shown that a side-on approach is favoured in the formation of the Ca$^+$–O$_2$ species,[3] which also exhibits charge transfer from Ca$^+$ to O$_2$. It might therefore be expected that a similar situation may arise for these complexes.

**Table 8.6.** Total energies, electronic states and harmonic vibrational frequencies for $O_2Ca^+$–X complexes (where X = $CO_2$, $N_2$ and $H_2O$) calculated at MP2/6-311++G (2d,p) level of theory.

| X | Y | State | Energy ($E_h$) | Vibrational frequencies (cm$^{-1}$) |
|---|---|---|---|---|
| $CO_2$ | $O_2$ | $^2A$ | -1015.153703 | 16(a), 32(a), 83(a), 85(a), 207(a), 512(a), 640(a), 640(a), 1063(a), 1283(a), 1327(a), 2420(a) |
| $N_2$ | $O_2$ | $^2A$ | -936.219998 | 16(a), 32(a), 162(a), 167(a), 192(a), 516(a), 1063(a), 1306(a), 2185(a) |
| $H_2O$ | $O_2$ | $^2A$ | -903.222454 | 14(a), 46(a), 191(a), 331(a), 410(a), 476(a), 523(a), 1062(a), 1324(a), 1666(a), 3763(a), 3862(a) |

**Table 8.7.** Total energies, electronic states, harmonic vibrational frequencies for $O_2Ca^+$–X complexes (where X = $CO_2$, $N_2$ and $H_2O$) calculated at B3LYP/6-311++G (2d,p) level of theory.

| X | Y | State | Energy ($E_h$) | Vibrational frequencies (cm$^{-1}$) |
|---|---|---|---|---|
| $CO_2$ | $O_2$ | $^2A$ | -1016.489272 | 37(a), 44(a), 83(a), 86(a), 205(a), 425(a), 516(a), 652(a), 653(a), 1185(a), 1369(a), 2432(a) |
| $N_2$ | $O_2$ | $^2A$ | -937.391057 | 41(a), 42(a), 158(a), 161(a), 181(a), 425(a), 522(a), 1185(a), 2448(a) |
| $H_2O$ | $O_2$ | $^2A$ | -904.322100 | 26(a), 55(a), 154(a), 323(a), 407(a), 420(a), 480(a), 524(a), 184(a), 1676(a), 3756(a), 3833(a) |

As before, calculations commenced with the individual species approaching from opposite sides of the $Ca^+$ in a linear orientation but, as observed with O–$Ca^+$–$CO_2$, this yielded structures with imaginary harmonic vibrational frequencies, indicating that these stationary points were saddle points on the potential energy surface. Again, geometry optimization symmetry constraints were relaxed and the various moieties were allowed to bend towards, as well as twist with respect to one another, this allowed the global minima to be located, as detailed in Tables 8.6 and 8.7. All of the lowest energy structures calculated for the $O_2$–$Ca^+$–X complexes, shown in Figure 8.1 are similar in that the approach by $O_2$ may be approximately described as

side-on in manner, whilst the favoured directions of approach by the second ligand is off-linear, resulting in a bent structure. As seen for previous species $CO_2$ and $N_2$ both favour an end-on approach, while $H_2O$ approaches *via* the δ- oxygen pointing towards the $Ca^+$ with the two hydrogens laying in the plane of the molecule. Of the two states studied, the doublet state was again the lowest in energy owing to charge transfer occurring in this spin state, evinced by analysis of spin and charge distributions in which the unpaired electron is shared between the two oxygen atoms of $O_2$. Consequently, these complexes can be viewed as $(CaO_2)^+$–L.

### 8.4.4  *Geometries of $O_2$–$Ca^+$–O Intermediate cluster ion.*

Of the complexes studied in the present paper, the $O_2$–$Ca^+$–O complex was the most challenging since O, $O_2$ and $Ca^+$ are all open-shell species. This results in the possibility of sextet, quartet and doublet spin states, as well as a variety of different structures. A comprehensive survey of these possibilities was performed, with the results of these shown in Table 8.8. The following considerations were taken into account. Firstly, there would be a strongly-bound O or $O_2$ moiety, owing to charge transfer from $Ca^+$, followed by the interaction of $O_2$ or O respectively. In the case of $O_2$ binding to $CaO^+$, the approach of $O_2$ could be side-on or linear, on the same, or opposite side to the O. Again in the case of O binding to $CaO_2^+$, the possibility that the approach of the O could be on the same or opposite side to the $O_2$ must be considered. Secondly, the lowest excited singlet state of O atoms ($^1D$) and of $O_2$ ($^1\Delta_g$) are significantly higher in energy than

the triplet states. With these considerations, doublet and sextet states should not arise in geometries where the ligands are on opposite sides of $Ca^+$ with the quartet states are expected (from the combinations of $CaO^+ + O_2$ and $CaO_2^+ + O$); however, for completeness these states were investigated. For the cases where all O atoms are on the same side of the complex, doublet or quartet states could arise. For these systems, a combination of B3LYP and MP2 calculations employing the 6-311++G(2d,p) basis sets were performed. However, in many MP2 calculations full geometry optimizations for all structures employing were not successful. A consistent set of data was obtained at the B3LYP level, therefore only these results are presented in Table 8.8.

**Table 8.8. Total energies, electronic states and harmonic vibrational frequencies for the $O_2Ca^+$–O complexes calculated at B3LYP/6-311++G (2d,p) level of theory. Note that $O_2$(s) indicates $O_2$ approaching in a side-on manner, whilst *i* indicates an imaginary frequency. The global minima are highlighted.**

| Complex | State | Energy ($E_h$) | Vibrational frequencies ($cm^{-1}$) |
|---|---|---|---|
| $sO_2$-$Ca^+$-O | $^4A_1$ | -902.950421 | $124i(b_2)$, $51i(b_1)$, $50(b_2)$, $91(a_1)$, $620(a_1)$, $1601(a_1)$ |
| $sO_2$-$Ca^+$-O | $^6B_2$ | -902.825906 | $122i(b_2)$, $30(b_1)$, $32(b_2)$, $33(a_1)$, $170(a_1)$, $1609(a_1)$ |
| $O_2$-$Ca^+$-O | $^4A$ | -902.956132 | $13(a)$, $79(a)83(a)$, $144(a)$, $619(a)$, $1623(a)$ |
| $O_2$-$Ca^+$-O | $^6\sum^+$ | -902.831321 | $11(\pi)$, $11(\pi)$, $48(\pi)$, $48(\pi)$, $113(\sigma)$, $185(\sigma)$, $1641(\sigma)$ |
| $O_2$-O-$Ca^+$ | $^2A_2$ | -902.931053 | $97i(b_2)$, $10i(b_1)$, $70(a_1)$, $107(b_2)$, $641(a_1)$, $1591(a_1)$ |
| $O_2$-O-$Ca^+$ | $^4B_1$ | -902.940352 | $46(a_1)$, $96(b_2)$, $155(b_1)$, $198(b_2)$, $698(a_1)$, $1615(a_1)$ |
| $O_3$-$Ca^+$ | $^2B_1$ | -902.984552 | $178(b_1)$, $298(b_2)$, $383(a_1)$, $687(a_1)$, $852(b_2)$, $1082(a_1)$ |
| $O$-$O_2$-$Ca^+$ | $^4B_1$ | -902.909116 | $39i(b_2)$, $32i(b_1)$, $48(a_1)$, $425(b_2)$, $525(a_1)$, $1188(a_1)$ |

| $CO_2$–$Ca^+$–$N_2$ | $CO_2$–$Ca^+$–$H_2O$ |
|---|---|
| $CO_2$–$Ca^+$–$O_2$ | $CO_2$–$Ca^+$–$O$ |
| $N_2$–$Ca^+$–$O_2$ | $H_2O$–$Ca^+$–$N_2$ |
| $H_2O$–$Ca^+$–$O_2$ | $O$–$Ca^+$–$N_2$ |
| $O$–$O_2$–$Ca^+$ | $O$–$Ca^+$–$H_2O$ |
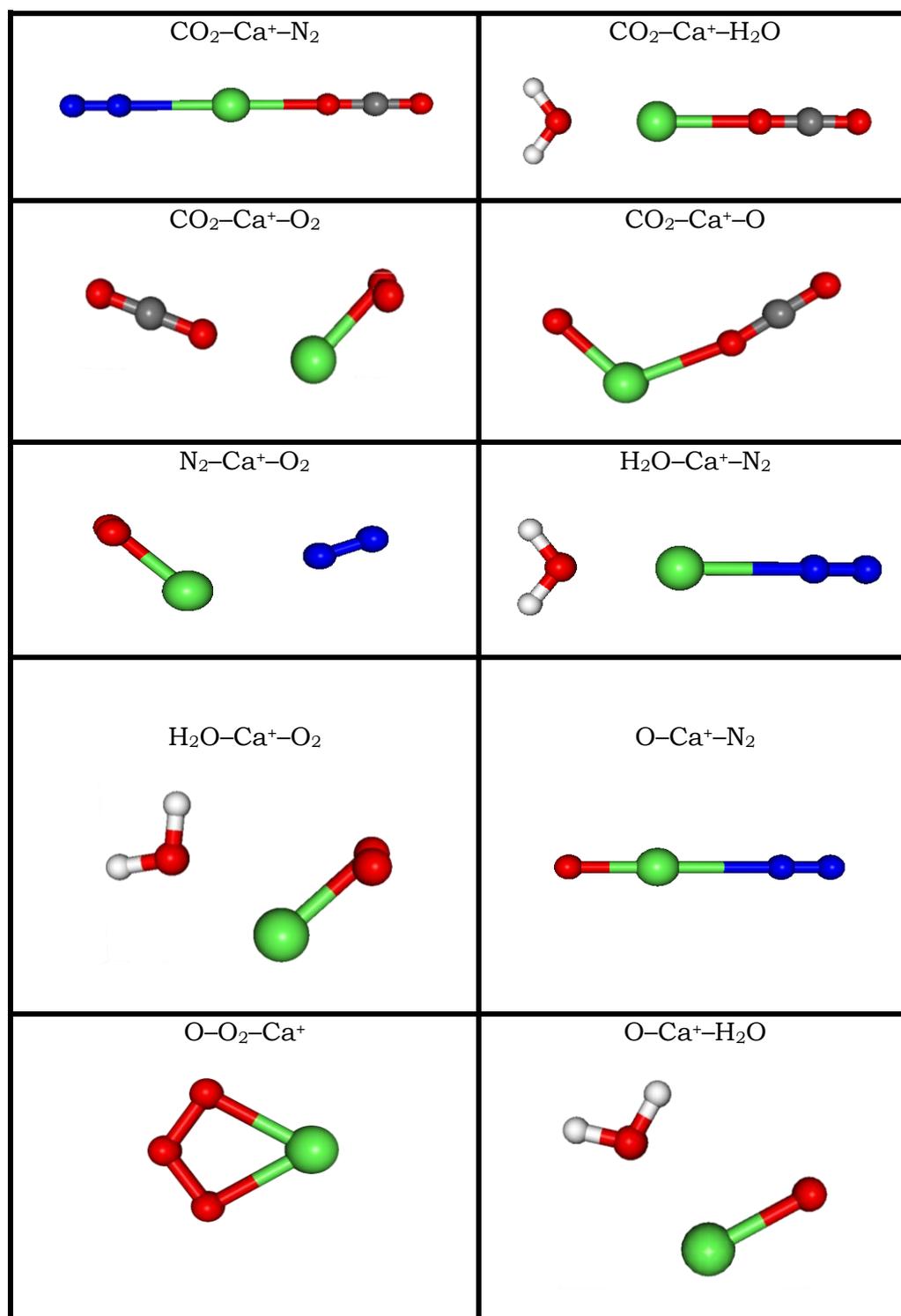
**Figure 8.1. B3LYP/6-311++G(2d,p) geometry optimized structures of Y–$Ca^+$–X complexes. Note that the lines joining atoms do not necessarily indicate a chemical bond.**

| O–Ca⁺–sO₂ (MP2) | O–Ca⁺–O₂ (B3LYP) |
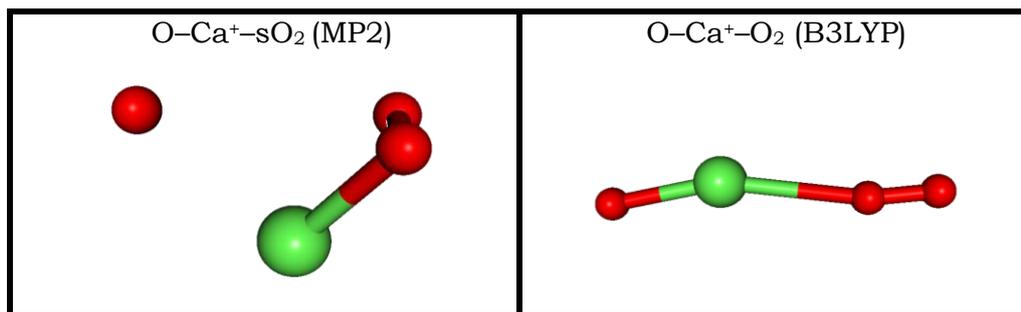
**Figure 8.2. Alternative B3LYP/6-311++G(2d,p) and MP2/6-311++G(2d,p) geometry optimized structures of O–Ca⁺–O₂ complexes. Note that the lines joining atoms do not necessarily indicate a chemical bond.**

From Table 8.8 it can be seen that the lowest energy structure for both methodologies is found for a doublet spin state ozonide structure, of the form $Ca^+–O_3$, which was the structure found previously.[3] A quartet state was searched for, initially in a linear orientation, which led to a saddle point, and hence an unconstrained search was undertaken at the B3LYP level, yielding a $C_1$ ($^4A$) structure, with the details given in Table 8.8. The analysis of the wavefunction showed this species to be $[(CaO^+)–O_2 (X^3\Sigma_g^-)]$. Interestingly, after some effort, the geometry of $[(CaO_2^+)–O(^3P)]$ at the MP2 level of theory was determined, again leading to a $^4A$ state (but this was found to lie higher in energy than the other $^4A$ state at the RCCSD(T) level). These structures represent approach of $CaO^+$ by $O_2$ and of O to $CaO_2^+$. The two structures are shown in Figure 8.2.

### 8.4.5 Ca⁺(X)₂ Complexes

Geometry optimizations and harmonic vibrational frequency calculations were also carried out for $Ca^+(N_2)_2$, $Ca^+(CO_2)_2$ $Ca^+(H_2O)_2$, and $Ca^+(O_2)_2$. In the first two cases, linear structures were obtained, giving real frequencies, in line with expectations based on the above

discussion for the mixed complexes, and the results on the Ca$^+$–X complexes.

For Ca$^+$(N$_2$)$_2$, similar calculations were performed on structures that had zero, one and two N$_2$ molecules side-on, with linear orientations for the other N$_2$; symmetry constraints were relaxed if required. The linear structure was the lowest in energy, followed by a slightly non-planar "T" shaped structure, with a planar "butterfly" (two N$_2$ molecules approaching side-on) the highest in energy. The results are presented in Table 8.9, with geometries shown in Figure 8.3.

**Table 8.9. Total energies, electronic states and harmonic vibrational frequencies for Ca$^+$(X)$_2$ complexes calculated at the B3LYP/6-311++G(2d,p) level. Note that sN$_2$ or sO$_2$ indicates N$_2$ or O$_2$ approaching in a side-on manner. The global minima are highlighted.**

| Complex | State | Energy ($E_h$) | Vibrational frequencies (cm$^{-1}$) |
|---|---|---|---|
| N$_2$–Ca$^+$–N$_2$ | $^2\Sigma^+$ | -896.496224 | 31($\pi_u$), 31($\pi_u$), 116($\sigma_g$), 137($\pi_g$), 137($\pi_g$), 167($\pi_u$), 167($\pi_u$), 179($\sigma_u$), 2447($\sigma_u$), 2447($\sigma_g$) |
| sN$_2$–Ca$^+$–sN$_2$ | $^2$A | -896.477328 | 37(a), 61(a), 131(a), 164(a), 198(a), 223(a), 347(a), 2041(a), 2179(a). |
| sN$_2$–Ca$^+$–N$_2$ | $^2$A'' | -896.485698 | 24(a'), 54(a''), 168(a'), 172(a'), 206(a''), 318(a'), 322(a''), 1947(a'), 2357(a') |
| O$_2$–Ca$^+$–O$_2$ | $^4$A | -978.197368 | 24(a), 32(a), 57(a), 59(a), 153(a), 428(a), 515(a), 1183(a), 1638(a) |
| CO$_2$–Ca$^+$–CO$_2$ | $^2\Sigma_g^+$ | -1054.692227 | 22($\pi_u$), 22($\pi_u$), 56($\pi_g$), 56($\pi_g$), 75($\pi_u$), 75($\pi_u$), 136($\sigma_g$), 233($\sigma_u$), 642($\pi_g$) |
| H$_2$O–Ca$^+$–H$_2$O | $^2$A$_1$ | -830.356761 | 42(a$_1$), 48(b$_2$), 54(a$_2$), 262(a$_1$), 323(a$_1$), 327(b$_2$), 337(b$_2$) 406(b$_1$), 413(a$_2$), 1648(b$_2$), 1651(a$_1$), 3730(a$_1$), 3731(b$_2$), 3813(a$_2$),3815(b$_1$) |

The complex with two water molecules gave a symmetric planar structure (see Figure 8.3), and the one with two CO$_2$ molecules was linear. For the O$_2$ dimer, a CaO$_2^+$ moiety was assumed, and the other

$O_2$ was allowed to approach from the opposite side, a quartet spin state minimum was found where the second $O_2$ slightly deviated from linear. See Table 8.9 and Figure 8.3 for details.

| $N_2$–$Ca^+$–$N_2$ | $sN_2$–$Ca^+$–$sN_2$ |
|---|---|
| $sN_2$–$Ca^+$–$N_2$ | $sO_2$–$Ca^+$–$O_2$ |
| $CO_2$–$Ca^+$–$CO_2$ | $H_2O$–$Ca$–$H_2O$ |
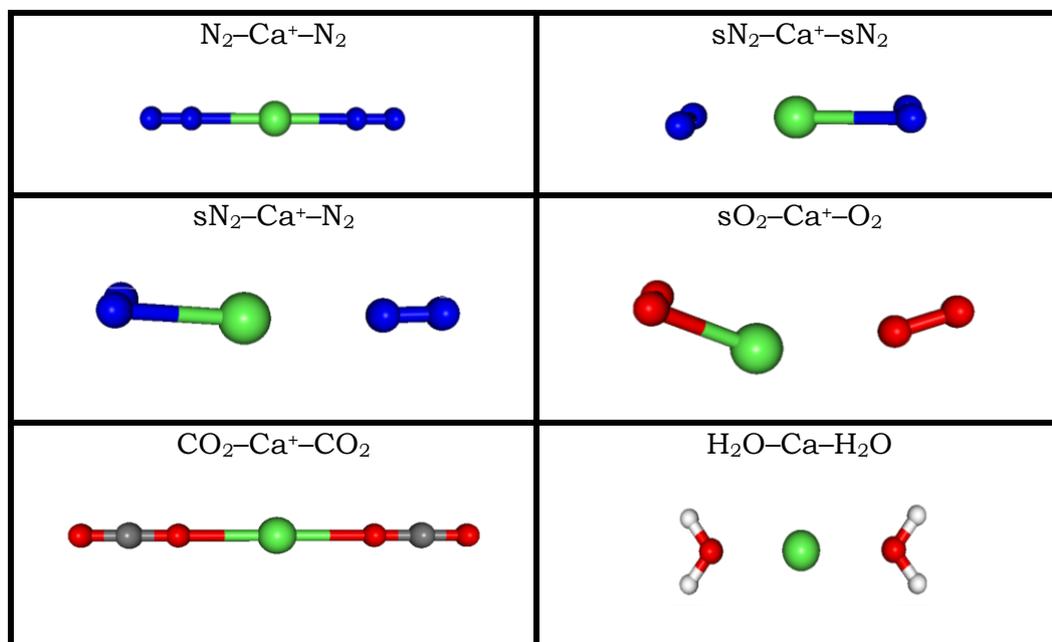
**Figure 8.3. B3LYP/6-311++G(2d,p) geometry optimized structures of Ca+(X)₂ complexes. Note that the lines joining atoms do not necessarily indicate a chemical bond.**

### 8.4.6  RCCSD(T) Calculations

In order to establish relative energetics more reliably, single point RCCSD(T) calculations were performed on both the B3LYP/6-311-G(2d,p) and MP2/6-311+G(2d,p) optimized geometries for a number of the Y–$Ca^+$–X complexes.  There was no consistent preference as to whether the B3LYP or MP2 structures were lower in energy, from the initial RCCSD(T) results, and so it was elected that the B3LYP optimized geometries would be used for all systems.  This meant that the $Ca^+$–X complexes did not need to be recalculated at the MP2 level and was also consistent with a very recent paper on potassium ions.[24]

**Table 8.10.  RCCSD(T)/aug-cc-pVQZ//B3LYP/6-311++G(2d,p) total energies and summary of lowest energy state and associated rotational constants.**

| Species | State | Energy/$E_h$ | Rotational Constants (GHz) |
|---|---|---|---|
| $CO_2$ | $^1\Sigma_g^+$ | -188.389566 | 0.0, 11.7, 11.7 |
| $H_2O$ | $^1A_1$ | -76.363530 | 825.4, 428.4, 282.0 |
| O | $^3P$ | -74.994931 | - |
| $O_2$ | $^3\Sigma_g^-$ | -150.177984 | 0.0, 43.3, 43.3 |
| $N_2$ | $^1\Sigma_g^+$ | -109.407028 | 0.0, 60.6, 60.6 |
| $Ca^+$ | $^2A_1$ | -676.790258 | - |
| $Ca^+–CO_2$ | $^2\Sigma^+$ | -865.202745 | 0.0, 0.0, 1.7 |
| $Ca^+–H_2O$ | $^2A_1$ | -753.198686 | 416.2, 7.1, 7.0 |
| $CaO^+$ | $^2\Sigma^{+\ (a)}$ | -751.907439 | 0.0, 0.0, 11.2 |
| $CaO_2^+$ | $^2A_2$ | -827.056718 | 5.9, 7.0, 35.6 |
| $Ca^+–N_2$ | $^2\Sigma^+$ | -786.207015 | 0.0, 0.0, 3.7 |
| $(CO_2)Ca^+(N_2)$ | $^2\Sigma^+$ | -974.618409 | 0.0, 0.6, 0.6 |
| $(CO_2)Ca^+(H_2O)$ | $^2A_1$ | -941.608032 | 415.8, 0.9, 0.9 |
| $(CO_2)Ca^+(O_2)$ | $^2A$ | -1015.479034 | 8.9, 0.9, 0.9 |
| $(CO_2)Ca^+(O)$ | $^2A'$ | -940.331720 | 12.5, 1.3, 1.2 |
| $(N_2)Ca^+(O_2)$ | $^2A$ | -936.483952 | 9.3, 1.6, 1.4 |
| $(N_2)Ca^+(H_2O)$ | $^2A_1$ | -862.613895 | 415.7, 1.3, 1.3 |
| $(O_2)Ca^+(H_2O)$ | $^2A$ | -903.474762 | 9.0, 3.2, 2.7 |
| $(N_2)Ca^+(O)$ | $^2\Sigma^+$ | -861.333304 | 0.0, 1.6, 1.6 |
| $(O_2)Ca^+(O)$ | $^4A$ | -902.100561 | |
| $CaO_3^+$ | $^2B_1$ | -902.136213 | 12.6, 4.9, 3.5 |
| $(H_2O)Ca^+(O)$ | $^2A''$ | -828.322184 | 13.2, 5.2, 3.7 |
| $Ca^+(N_2)_2$ | $^2\Sigma^+$ | -895.623276 | 0.0, 1.0, 1.0 |
| $Ca^+(CO_2)_2$ | $^2\Sigma_g^+$ | -1053.612999 | 0.0, 0.4, 0.4 |
| $Ca^+(H_2O)_2$ | $^2A_1$ | -829.602621 | 208.2, 2.4, 2.4 |
| $Ca^+(O_2)_2$ | $^4A$ | - | 17.5, 1.2, 1.2 |

a  Recent calculations and previous work[15] suggest that actual ground state is $^2\Pi$.

In Table 8.10 the RCCSD(T)/aug-cc-pVQZ//B3LYP/6-311++G(2d,p) energies for the species under consideration are presented, from which the binding energies in Table 8.8 can be derived.  There only appears to be experimental data for the $Ca^+(H_2O)_2$ complex,[9] with a derived binding energy of 100 kJ mol$^{-1}$, which compares well with the value of 106 kJ mol$^{-1}$ determined in the present study.  A previous HF calculation yielded[9] a value of 97 kJ mol$^{-1}$, which is in good agreement with the much higher-level value here.  It is interesting to note that

the removal of the second water (54.3 kJ mol$^{-1}$) is easier than the first (111.1 kJ mol$^{-1}$), attributable to the solvation of the Ca$^+$ by the first water, and indeed this trend in lowering of dehydration energies continues for larger complexes.[9] For the other complexes, it is a general finding that the energy required to remove a ligand from a ligated Ca$^+$-complex is smaller than from Ca$^+$. Unfortunately, there were problems obtaining convergence with the RCCSD(T) calculation on Ca$^+$(O$_2$)$_2$, but since this was not of importance for the modelling calculations, this was not pursued further.

**Table 8.11. Binding Energies for X–Ca$^+$–Y Complexes (kJ mol$^{-1}$)**

| Species | Removal of X | Removal of Y |
|---|---|---|
| $CO_2$–Ca$^+$–N$_2$ | 57.3 | 22.7 |
| $CO_2$–Ca$^+$–H$_2$O | 51.9 | 109.6 |
| $CO_2$–Ca$^+$–O$_2$ | 86.0 | 258.1 |
| $CO_2$–Ca$^+$–O | 91.1 | 351.9 |
| N$_2$–Ca$^+$–O$_2$ | 53.0 | 259.8 |
| N$_2$–Ca$^+$–H$_2$O | 21.5 | 113.8 |
| O$_2$–Ca$^+$–H$_2$O | 257.5 | 143.1 |
| N$_2$–Ca$^+$–O | 49.4 | 344.9 |
| O$_2$–Ca$^+$–O | 39.7 | 128.4 |
| H$_2$O–Ca$^+$–O | 134.5 | 337.5 |
| N$_2$–Ca$^+$–N$_2$ | 24.2 | 24.2 |
| $CO_2$–Ca$^+$–$CO_2$ | 106.1 | 106.1 |
| H$_2$O–Ca$^+$–H$_2$O | 54.3 | 54.3 |

## 8.5  Conclusions

Accurate binding energies for the Ca$^+$–X complexes have been obtained, and these are in agreement with previous experimental data where available. $D_0$ values for Ca$^+$–H$_2$O and Ca$^+$–N$_2$ were in good agreement with experiment, but the value for Ca$^+$–$CO_2$ was very much higher than determined experimentally, but the latter value had been

noted by the authors as being an extreme lower bound.[13]  It was also shown that the value for $CaO_2^+$ was in line with known data.

For the complexes with two ligands, it can be seen that each species for which there are a number of possible structures, there is a preferred direction of approach, independent of the other ligand present in the complex.  $N_2$ and $CO_2$ both prefer to approach end-on while $O_2$ prefers to approach the calcium cation side-on.  In all the complexes studied it has been shown that the complex will be most stable in its lowest spin multiplicity state.  In the case of complexes involving O and $O_2$, this is achieved by the formation of a chemical bond, *via* the donation of an electron from $Ca^+$ to O or $O_2$; essentially forming $Ca^{2+}$ and $O^-$ or $O_2^-$ ions, and hence forming doublet species in preference to the quartet.  In these O or $O_2$ species, the complex formed was in most cases bent, allowing a greater interaction between $\delta-$ parts of the other ligand and the $Ca^{2+}$, and a greater interaction of $\delta+$ parts of the other ligand and the negative charge on the $O^-$ or $O_2^-$. The binding energies for the removal of one ligand from a complex consisting of two ligands may be seen to be generally slightly smaller than for the removal of the same ligand from $Ca^+$.

The results of these calculations have since been used to model experimental studies of the kinetics of second ligand-switching reactions of $Ca^+$ molecular ions.[2]  In light of more recent calculations on the $Ca^+O$ complex suggesting a $^2\Pi$ ground state, further calculations are required to determine the effect that this would have on the chemistry of calcium in this region of the atmosphere.

# References

[1] J. M. Grebowsky and A. C. Aikin, In *Meteors in the Earth's Atmosphere*; E. Murad, I. P. Williams, Cambridge University Press, Cambridge, 2002.

[2] S. L. Broadley, T. Vondrak, T. G. Wright and J. M. C. Plane, *Phys. Chem. Chem. Phys.,* 2008, **10**(34), 5287.

[3] S. L. Broadley, T. Vondrak and J. M. C. Plane, *Phys. Chem. Chem. Phys.*, 2007, **9**(31), 4357.

[4] M. J. Frisch, G. W. Trucks, H. B. Schlegel, G. E. Scuseria, M. A. Robb, J. R. Cheeseman, J. A. Montgomery, Jr., T. Vreven, K. N. Kudin, J. C. Burant, J. M. Millam, S. S. Iyengar, J. Tomasi, V. Barone, B. Mennucci, M. Cossi, G. Scalmani, N. Rega, G. A. Petersson, H. Nakatsuji, M. Hada, M. Ehara, K. Toyota, R. Fukuda, J. Hasegawa, M. Ishida, T. Nakajima, Y. Honda, O. Kitao, H. Nakai, M. Klene, X. Li, J. E. Knox, H. P. Hratchian, J. B. Cross, V. Bakken, C. Adamo, J. Jaramillo, R. Gomperts, R. E. Stratmann, O. Yazyev, A. J. Austin, R. Cammi, C. Pomelli, J. Ochterski, P. Y. Ayala, K. Morokuma, G. A. Voth, P. Salvador, J. J. Dannenberg, V. G. Zakrzewski, S. Dapprich, A. D. Daniels, M. C. Strain, O. Farkas, D. K. Malick, A. D. Rabuck, K. Raghavachari, J. B. Foresman, J. V. Ortiz, Q. Cui, A. G. Baboul, S. Clifford, J. Cioslowski, B. B. Stefanov, G. Liu, A. Liashenko, P. Piskorz, I. Komaromi, R. L. Martin, D. J. Fox, T. Keith, M. A. Al-Laham, C. Y. Peng, A. Nanayakkara, M. Challacombe, P. M. W. Gill, B. G. Johnson, W. Chen, M. W. Wong, C. Gonzalez and J. A. Pople, GAUSSIAN 03 (Revision B.03), Gaussian, Inc., Wallingford, CT, 2003.

[5] MOLPRO is a package of ab initio programs written by H.-J. Werner, P. J. Knowles and others.

[6] J. Koput and K. A. Peterson, *J. Phys. Chem. A,* 2002, **106**, 9595.

[7] F. Jensen, Introduction to computational chemistry Second Edition, John Wiley & Sons Ltd., Chichester, 2007.

[8] C. W. Bauschlicher, Jr., H. Partridge, M. Sodpupe and S. R. Langhoff, *J. Phys. Chem.,* 1992, **96**, 9259.

[9] E. Kochanski and E. Constantin, *J. Chem. Phys.* 1987, **87**, 1661.

[10] S. H. Pullins, J. E. Reddic, M. R. France and M. A. Duncan, *J. Chem. Phys,* 1998, **108**, 2725.

[11] K. N.Kirschner, B. Ma, J. P. Bowen and M. A. Duncan, *Chem. Phys. Letts.* 1998, **295**, 204.

[12] L. Rodriguez-Santiago and C. W. Buschlicher Jr., C. W. *Spectrochim. Acta A,* 1999, **55**(3), 457.

[13] C. T. Scurlock, S. H. Pullins and M. A. Duncan, *J. Chem. Phys.,* 1996 **105**, 3579.

[14] R. J. Plowright, T. G. Wright and J. M. C. Plane, *J. Phys. Chem. A,* 2008, **112**, 6550.

[15] J. F. Harrison, R. W. Field and C. C Jarrold, *ACS Symposium Ser.* 2002, **828**, 238.

[16] T. G. Wright, A. M. Ellis and J. M. Dyke, *J. Chem. Phys.,* 1993, **98**(4), 2891.

[17] D. R. Herschbach, C. E. Klob, D. R. Worsnop and X. Shi, *Nature,* 1992, **356**, 414.

[18] X. Shi, D. R. Herschbach, D. R. Worsnop and C. E. Klob, *J. Phys. Chem.,* 1993, **97**(10), 2113.

[19] H. Partidge, S. R. Langhoff and C. W. Bauschlicher Jr., *J. Chem. Phys.,* 1986, **84**, 4489.

[20] E. R. Fisher, J. L. Elkind, D. E. Clemmer, R. Georgiadis, S. K. Loh, N. Aristov, L. S. Sunderlin and P. B. Armentrout, *J. Chem. Phys.* 1990, **93**, 2676.

[21] E. Murad, *J. Chem. Phys.* 1983, **78**, 6611.

[22] E. P. F. Lee, Z.Almahdi, A. Musgrave and T. G. Wright, *Chem. Phys. Lett.,* 2003, **373**, 599.

[23] P. Soldán, E. P. F. Lee, S. D. Gamblin and T. G. Wright, *Chem. Phys. Lett.*, 1999, **313**, 379.

[24] J. M. C. Plane, R. J. Plowright and T. G. Wright, *Journal of Physical Chemistry A,* 2006, **110***,* 3093*.*